Thermal Analysis of Processes at the Solid-Phase Synthesis of Lithium-Titanium Ferrite

E. V. Nikolaev[a],*, E. N. Lysenko[a], and A. P. Surzhikov[a]

[a]Tomsk Polytechnic University, Tomsk, 634050 Russia
*e-mail: nikolaev0712@gmail.com

Abstract—In this study, the reactivity of a Fe_2O_3—Li_2CO_3—TiO_2 mixture with different initial densities was investigated by thermal and kinetic methods to analyze phase formation of lithium titanium ferrite. Test samples were powder with a density of 1 g/cm^3 and a compact with a density of 2.6 g/cm^3. High-density samples were formed by single-action cold compaction. It is shown that the reaction of solid-phase interaction of lithium-titanium ferrite strongly depends on the degree of compaction. The mass of the powder mixture sample decreases in the temperature range of 500—720°C. In compacts, the reaction of solid-phase interaction starts at lower temperature (~420°C). In addition, it is shown that in compacted samples, a lithium ferrite spinel phase is formed during heating. The kinetic analysis was used to determine the kinetic model of the synthesis reaction of lithium-titanium ferrite and to calculate the parameters of this process.

INTRODUCTION

Ferrites are compounds of iron oxide Fe_2O_3 with other metals oxides. Hundreds of different types of ferrites currently used differ in chemical composition, crystal structure, magnetic, electrical and other properties. Spinel ferrites have become most widely used [1—3].

Lithium ferrites, in which Fe^{3+} ions [4] are replaced by titanium ions, are widely used in microwave, electronics and other fields. In addition, these compounds can be used to replace other ferrites due to their good magnetic and electrical properties [5—7]. Among a number of methods used to synthesize lithium ferrites, the most common is the method based on high-temperature solid-phase interaction of compacted powders [8—10]. However, this method has a number of significant limitations in synthesis of lithium ferrites. These limitations include low thermal stability of some of the initial reagents and incomplete synthesis reaction caused by heating. These negative factors can led to decrease chemical and structural uniformity of the final product. Thus, for efficient production of ferrite materials, various methods are used to increase the degree of homogenization and to activate the reaction mixtures, which accelerate solid-phase interaction due to lower synthesis temperature.

There are a number of chemical methods used to increase the degree of homogenization of reaction mixtures. These methods typically include: precipitation of salts or hydroxides [11], spray pyrolysis [12], combustion [13, 14], and sol-gel technology [15]. It should be noted that the effectiveness of these methods is limited due to their complexity and low potential for industrial production.

On the other hand, it is known that a solid-solid chemical reaction does not proceed in the entire volume of solid particles that chemically interact with each other, but in the contact zones between reacting particles. Thus, the number of contacts between reacting particles and their contact area strongly affect the initial stage of solid-phase synthesis. One of the effective methods to increase the number of contacts in the initial reaction mixtures is mechanical treatment of powder reagents in high-energy planetary mills [16—18]. In our previous studies, the effect of mechanical treatment of the initial mixture on ferrite production at a lower synthesis temperature was shown in detail [19, 20]. However, the effect of the density of the initial mixture on synthesis without pre-treatment was considered for $Li_{0.5}Fe_{2.5}O_4$ lithium ferrite only.

Therefore, in this study, lithium-titanium ferrite was synthesized to investigate the effect of the reactivity of the initial powders with different initial densities on the solid-phase interaction. For the experiment, samples with bulk densities of 1 and 2.6 g/cm^3 were compacted at 0 and 200 MPa, respectively. In addition, a kinetic model and parameters describing synthesis of lithium titanium ferrite from powder and compacted samples were obtained using kinetic anal-
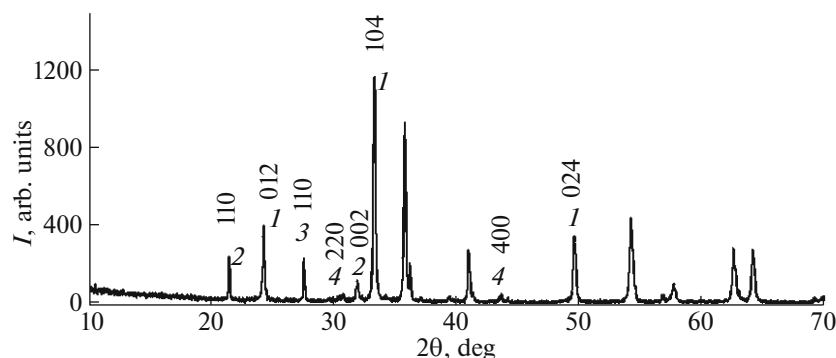
Fig. 1. XRD pattern for initial $Li_2CO_3 + Fe_2O_3 + TiO_2$ mixture ((1) Fe_2O_3, (2) Li_2CO_3, (3) TiO_2, (4) spinel).

ysis. Kinetic analysis was performed on the basis of the data obtained in thermal analysis of the reaction mixtures.

EXPERIMENTAL

As initial reagents, industrial powders Fe_2O_3, TiO_2 (analytically pure), Li_2CO_3 (chemically pure) were used. The initial reagent powders were pre-dried in the laboratory oven at 200°C. The ratio of the initial reagents in the powder mixtures was calculated by the equation:

$$0.99Li_2CO_3 + 3.63Fe_2O_3 + 0.66TiO_2 \\ \rightarrow 3.3Li_{0.6}Fe_{2.2}Ti_{0.2}O_4 + 0.99CO_2\uparrow. \quad (1)$$
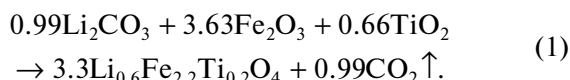
After that, the mixture of the initial reagents $Li_2CO_3-Fe_2O_3-TiO_2$ was divided into two parts. The first part was studied in the form of powder with a bulk density of 1 g/cm³ (S1 sample). The second part consisted of pellets with a diameter of 9 mm and a thickness of 2 mm compacted by single-action cold compaction. The samples were compacted at 200 MPa for 3 min using a PGR-10 hydraulic press. The sample density was 2.6 g/cm³ (S2 sample).

Structural parameters of the initial powders were evaluated by XRD analysis using an ARL X'TRA diffractometer (Switzerland). Figure 1 shows the XRD pattern for the mixture of the initial reagents to produce lithium-titanium ferrites: α-Fe_2O_3 (PDF no. 40-

Table 1. Structural parameters and phase composition obtained by XRD analysis

Phase	Lattice parameter, Å	Crystallite size, nm	$(\Delta d/d) \times 10^3$
α-Fe_2O_3	$a = b = 5.033, c = 13.753$	89	0.6
Li_2CO_3	$a = 8.259, b = 4.974, c = 6.198$	159	0.3
TiO_2	$a = b = 4.594, c = 2.959$	74	0.4
γ-Fe_2O_3	$a = b = c = 8.344$	42	1.5

142), Li_2CO_3 (PDF no. 66-941), and TiO_2 (PDF no. 82-656).

The peaks at $2\theta \approx 30.3°$ and $43°$ correspond to the spinel phase γ-Fe_2O_3 (PDF no. 79-196), which is usually added in a small amount of ~1 wt % to iron oxide to synthesize lithium ferrites. Structural parameters, the crystallite size, and the values of internal elastic microstresses ($\Delta d/d$) of the samples were determined using the Powder Cell software. These data are summarized in Table 1.

Thermal analysis of the test samples was performed using a STA 449C Jupiter synchronous thermal analyzer (Netzsch, Germany) with weight sensitivity of ~0.1 μg. The samples were placed into corundum crucibles (Al_2O_3) and studied in air. Heating up to 800°C was performed at different heating rates in the range of (2.5−20)°C/min. Proteus Analysis and Thermokinetics software was used to process the data from thermal analysis. In addition, Thermokinetics software was used for kinetic analysis.

RESULTS AND DISCUSSION

Figure 2 shows the results of thermal analysis for samples with different initial densities. The behavior of the thermogravimetric curve (TG-curve) at the heating stage for S1 and S2 samples corresponds to the process of lithium-titanium ferrite synthesis. Regardless of the initial density of the reaction mixture, the TG-curves show mass loss. In S1 sample, mass loss starts at ~500°C. The behavior of the differential thermogravimetric curve (DTG-curve) indicates that this process consists of two stages. The first stage is characterized by interaction of the initial oxides and carbonate in the mixture followed by decomposition of Li_2CO_3 in the temperature range of 550−680°C, and the second stage involves melting of lithium carbonate residues at ~723°C.

The DTG curve repeats the shape of the differential scanning calorimetry (DSC) curve, which shows that the change in mass can be attributed to the endothermic effect (87 J/g) occurring in the temperature
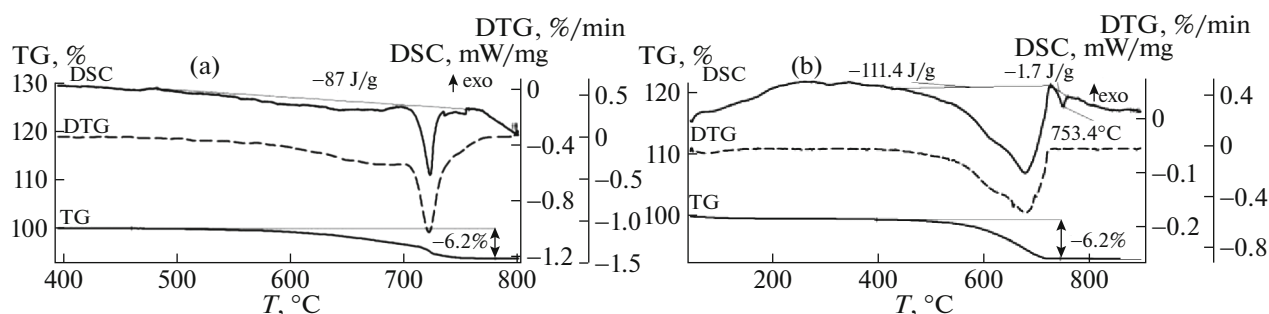
Fig. 2. Thermal analysis data for (a) S1 and (b) S2 samples.

range of 500–720°C. The TG-curve was used to calculate the mass loss during heating, which was 6.2 ± 0.1%. This value correlates well with the theoretical value of the mass loss according to Eq. (1). A slightly different picture can be observed for S2 samples with a density of 2.6 g/cm^3 (Fig. 2b). The main mass loss in heating starts at ~420°C, which is 80°C less than that for S1 samples. The total mass change was 6.2 ± 0.1%. The DSC curve shows an endothermic peak of 111 J/g, which corresponds to the mass loss in the range of 430–720°C. An insignificant endothermic peak (1.7 J/g) observed at 753°C is characteristic of α → β phase transition in Li$_{0.5}$Fe$_{2.5}$O$_4$ ferrite. This transition phase is formed during synthesis of lithium-substituted ferrospinels, including lithium-titanium ferrites.

A comparison of the TG/DSC curves for samples with different initial densities (Fig. 2) shows that the solid-phase interaction in the Fe$_2$O$_3$–Li$_2$CO$_3$–TiO$_2$ system strongly depends on the powder mixture density. Compacted S2 samples exhibit the spinel phase of lithium ferrite formed upon heating. As shown for pure lithium ferrite, the DSC peak observed in this phase transition is ~13 J/g [21]. It should be assumed that only ~13% of the lithium ferrite phase can be formed under these conditions.

TG data were used to perform kinetic analysis of lithium-titanium ferrite synthesis. TG curves were measured at different heating rates: 2.5, 5, 10, and 20°C/min in non-isothermal mode. As is known [22, 23], the main goal of kinetic analysis is to describe the reaction of solid-phase interaction by mathematical methods and to find a model and parameters that can best describe the process. A kinetic model and corresponding parameters are used to optimize technological modes of thermal synthesis [24, 25]. The kinetic analysis equation is generally represented as follows:

$$d\alpha/dt = k f(\alpha), \qquad (2)$$

where α is conversion degree, $f(\alpha)$ is the temperature-independent function of the conversion ratio, and k is the rate constant which can be expressed by Arrhenius equation:

$$k = A \exp\left(-\frac{E_a}{RT}\right), \qquad (3)$$

where A is a pre-exponential factor, E_a is activation energy, T is an absolute temperature, and R is the gas constant (8.314 J K^{-1} mol^{-1}).

The following equation is the final expression for the rate of the thermal decomposition process:

$$d\alpha/dt = kf(\alpha) = Af(\alpha)\exp\left(-\frac{E_a}{RT}\right). \qquad (4)$$

Equation (3) is basic for kinetic analysis. The first stage in the kinetic analysis is application of the model-independent Friedman method [26] to estimate kinetic parameters. The Friedman (FR) method allows estimation of E_a and A in Arrhenius equation (3) without selecting a kinetic model of the reaction $f(\alpha)$. The FR method can be used to calculate E_a directly from the experimental temperature dependence of the conversion degree (α) obtained at different heating rates. The FR method is a linear differential method [27]. The results of the model-independent parameter estimation are presented in the form of dependences of the Arrhenius parameters (E_a and A), depending on the conversion degree α in the range from 0 to 1. Figure 3 shows the results of the FR analysis for S1 and S2 samples, respectively.

As can be seen in Fig. 3, the kinetic parameters strongly depend on the conversion degree in the entire range, which indicates that synthesis is described in a number of stages regardless of the reaction mixture density. The shape of the activation energy curves for S1 and S2 samples indicates that synthesis of lithium titanium ferrite has a two-stage mechanism with different kinetic parameters. Thus, it can be assumed that the multidimensional nonlinear regression method is required to determine a suitable kinetic model and kinetic parameters of thermal synthesis of lithium-titanium ferrite. This method provides a reaction model and Arrhenius parameters for each of the stages of thermal synthesis.

Thermokinetics software helped identify that the best simulation results for TG curves and mathematical models were obtained using the two-stage mecha-
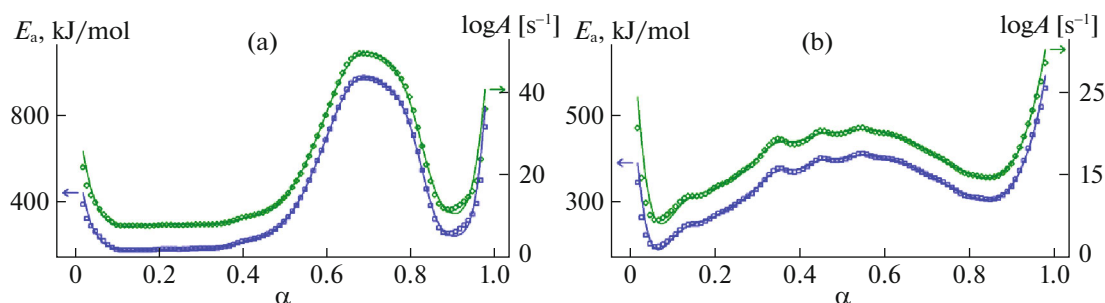
Fig. 3. Results of the Friedman analysis for (a) S1 and (b) S2 samples.
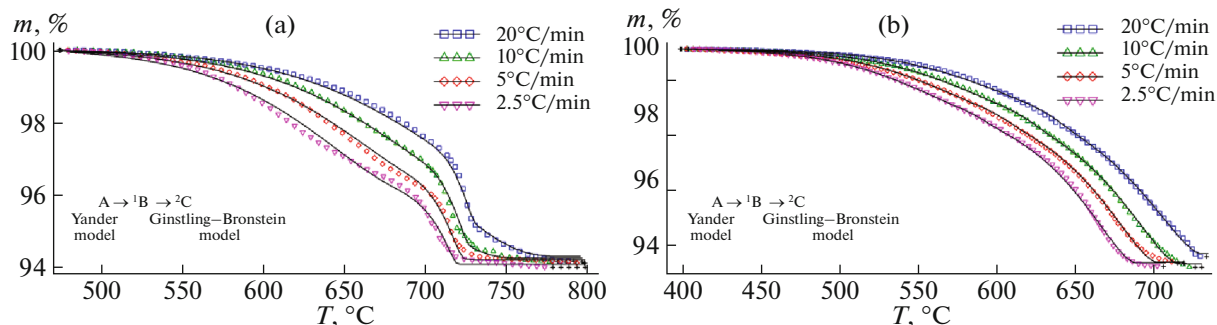

Fig. 4. Results of nonlinear-regression for (a) S1 and (b) S2 samples (lines indicate model curves, and symbols indicate experimental points).

nism $A \rightarrow {}^1B \rightarrow {}^2C$ (where $A \rightarrow B$ is synthesis stage 1, $B \rightarrow C$ is synthesis stage 2). Table 2 presents several well-known kinetic models used to perform mathematical modeling.

Figure 4 shows the results of kinetic analysis by nonlinear regression for both types of samples, and the calculated kinetic parameters are summarized in Table 3. The best results for S1 sample (Fig. 4a) were obtained using the Yander diffusion model (D3) at synthesis stage 1, and Ginstling−Brounstein model showed best results at stage 2 (D4).

These models (D3 → D4) were used to calculate the kinetic parameters. The activation energy at stage 1 is $E_a = 272$ kJ/mol. This high value may be due

to decomposition of lithium carbonate after heating. At stage 2, the activation energy increases significantly and attains 708 kJ/mol, which is probably associated with melting of unreacted lithium carbonate residues at ~720°C in accordance with thermal analysis. In addition, these values of the kinetic parameters correlate well with the Arrhenius parameters obtained by the FR method (Fig. 3a)

For samples with higher density (S2), lithium-titanium ferrite synthesis can be described as a two-stage mechanism, using the Yander and Ginstling−Brounstein models at both stages (Fig. 4b). The activation energies of ~258 and 380 kJ/mol obtained using multidimensional nonlinear regression for both stages (Table 3) are in good compliance with the values obtained by the FR method (Fig. 3b).

The activation energy at stage 1 is slightly lower, but comparable with the value of E_a for S1 sample at this stage. After that, the activation energy increases, but it has a value much lower than that for S1 sample. This can be due to a greater number of contacts between the reactants in the reaction mixture powders after compacting. In such samples, particles interact at the atomic level. Therefore, solid-phase interaction can occur at lower temperatures and with less energy. It should be noted that the performed calculations of kinetic parameters are characterized by a high correlation coefficient (~0.9997).

Table 2. Some types of models for kinetic analysis

Symbol	$f(\alpha)$	Reaction type
F1	e	First-order reaction
F2	e^2	Second-order reaction
Fn	e^n	nth-Order reaction
D1	$0.5/(1-e)$	One-dimensional diffusion
D2	$-1/\ln(e)$	Two-dimensional diffusion
D3	$1.5e^{1/3}/(e^{-1/3}-1)$	Three-dimensional diffusion (Jander's type)
D4	$1.5e/(e^{-1/3}-1)$	Three-dimensional diffusion (Ginstling−Brounstein type)

Table 3. Values of the kinetic parameters for studied samples

Sample	$\log A_1$ [s^{-1}]	E_{a1}, kJ/mol	$\log A_2$ [s^{-1}]	E_{a2}, kJ/mol	α
S1	14.8 ± 0.2	272 ± 3.3	35.7 ± 0.6	708 ± 4.4	0.69 ± 0.01
S2	12.5 ± 0.1	258 ± 1.3	17.5 ± 0.2	380 ± 1.3	0.31 ± 0.01

CONCLUSIONS

The effect of the initial density of the Fe_2O_3–Li_2CO_3–TiO_2 mixture on the solid-phase synthesis of lithium-titanium ferrites was studied using thermal and kinetic analyzes. Thermal analysis showed that a significant decrease in mass is characteristic of both types of samples and is associated with decomposition of lithium carbonate and interaction of oxides upon heating. In addition, this interaction proceeds in two stages for both types of samples. It should be noted that the solid-phase interaction reaction for S2 samples starts at lower temperatures. In addition, the calorimetric curves shows formation of a small amount of lithium ferrite $Li_{0.5}Fe_{2.5}O_4$, which indicates the main difference of samples (S2) compacted at 200 MPa.

Thermogravimetric curves obtained at different heating rates and Netzsch Thermokinetics software were used to perform kinetic analysis of lithium titanium ferrite synthesis. The results of kinetic analysis showed that solid-phase interaction is a diffusion reaction. It is shown that synthesis of both samples is best described by a two-stage mechanism $(A \rightarrow {}^1B \rightarrow {}^2C)$. Regardless of the method of sample production, Yander's and Ginstling–Brounstein diffusion models were applied at stages 1 and 2, respectively. The activation energy and pre-exponential factor in synthesis of compacted ferrite samples were shown to significantly decrease.

REFERENCES

1. M. Sharif, J. Jacob, M. Javed, A. Manzoor, K. Mahmood, and M. A. Khan, Phys. B (Amsterdam, Neth.) **567**, 45 (2019).

2. S. A. Mazen and N. I. Abu-Elsaad, Appl. Nanosci. **5**, 105 (2015).

3. J. Guo, H. Zhang, Z. He, S. Li, and Z. Li, J. Mater. Sci. Mater. Electron. **29**, 2491 (2018).

4. J. S. Kounsalye, P. B. Kharat, D. N. Bhoyar, and K. M. Jadhav, J. Mater. Sci. Mater. Electron. **29**, 8601 (2018).

5. Y. Gao, Z. Wang, R. Shi, H. Zhang, and X. Zhou, J. Alloys Compd. **805**, 934 (2019).

6. M. Kavanlooee, B. Hashemi, H. Maleki-Ghaleh, and J. Kavanlooee, J. Electron. Mater. **41**, 3062 (2012).

7. Q. Yin, Y. Liu, Q. Liu, Y. Wang, J. Chen, H. Wang, C. Wu, and H. Zhang, J. Mater. Sci.: Mater. Electron. **30**, 5430 (2019).

8. R. Guo, Z. Yu, Y. Yang, K. Sun, C. Wu, H. Liu, X. Jiang, and Z. Lan, J. Supercond. Nov. Magn. **30**, 1767 (2017).

9. S. S. Teixeira, M. F. Graça, and L. C. Costa, J. Non-Cryst. Solids **358**, 1924 (2012).

10. J. Hreŝĉak, B. Maliĉ, J. Cilenšek, and A. Benĉan, J. Therm. Anal. Calorim. **127**, 129 (2017).

11. Y. Wang, L. Yang, Y. Zhang, H. Zhang, and J. Wei, Russ. J. Phys. Chem. A **93**, 2771 (2019).

12. D. Kotsikau, M. Ivanovskaya, V. Pankov, and Y. Fedotova, Solid State Sci. **39**, 69 (2015).

13. V. Rathod, A. V. Anupama, V. M. Jali, V. A. Hiremath, and B. Sahoo, Ceram. Int. **43**, 14431 (2017).

14. V. Rathod, A. V. Anupama, R. Vijaya Kumar, V. M. Jali, and B. Sahoo, Vibr. Spectrosc. **92**, 267 (2017).

15. M. V. Berezhnaya, I. Y. Mittova, N. S. Perov, O. V. Al'myasheva, A. T. Nguyen, V. O. Mittova, V. V. Bessalova, and E. L. Viryutina, Russ. J. Inorg. Chem. **63**, 742 (2018).

16. V. Berbenni, G. Bruni, C. Milanese, A. Girella, and A. Marini, J. Therm. Anal. Calorim. **133**, 413 (2018).

17. T. T. Parlak, F. Apaydin, and K. Yildiz, J. Therm. Anal. Calorim. **127**, 63 (2017).

18. M. Kavanlooee, B. Hashemi, H. Maleki-Ghaleh, and J. Kavanlooee, J. Electron. Mater. **41**, 3082 (2012).

19. E. N. Lysenko, E. V. Nikolaev, A. P. Surzhikov, S. A. Nikolaeva, and I. V. Plotnikova, J. Therm. Anal. Calorim. **138**, 2005 (2019).

20. E. N. Lysenko, E. V. Nikolaev, A. P. Surzhikov, and S. A. Nikolaeva, Mater. Chem. Phys. **239**, 122055 (2020).

21. E. N. Lysenko, T. S. Frangulyan, A. P. Surzhikov, and S. A. Ghyngazov, J. Therm. Anal. Calorim. **108**, 1207 (2012).

22. P. Saikia, N. Blaise Allou, A. Borah, and R. L. Goswamee, Mater. Chem. Phys. **186**, 52 (2017).

23. J. Opfermann, J. Therm. Anal. Calorim. **60**, 641 (2000).
https://doi.org/10.1023/A:1010167626551

24. E. N. Lysenko, E. V. Nikolaev, and A. P. Surzhikov, IOP Conf Ser.: Mater. Sci. Eng. **110**, 012092 (2016).

25. P. Sharma and P. Uniyal, J. Therm. Anal. Calorim. **128**, 875 (2017).

26. A. Zh. Sarsenbekova, G. K. Kudaibergen, M. Zh. Burkeev, and G. K. Burkeeva, Russ. J. Phys. Chem. A **93**, 1252 (2019).

27. M. Erceg, I. Krešic, M. Jakic, and B. Andričic, J. Therm. Anal. Calorim. **127**, 789 (2017).